Implications of recent multimodel attribution studies for climate sensitivity

Nicholas Lewis[1]

Equilibrium Climate Sensitivity (ECS) is inferred from estimates of instrumental-period warming attributable solely to greenhouse gases (AW), as derived in two recent multi-model Detection and Attribution (D&A) studies that apply optimal fingerprint methods with high spatial resolution to 3D global climate model simulations. This approach minimises the key uncertainty regarding aerosol forcing without relying on low-dimensional models. The "observed" AW distributions from the D&A studies together with an observationally-based estimate of effective planetary heat capacity (EHC) are applied as observational constraints in (AW, EHC) space. By varying two key parameters – ECS and effective ocean diffusivity – in an energy balance model forced solely by greenhouse gases, an invertible map from the bivariate model parameter space to (AW, EHC) space is generated. Inversion of the constrained (AW, EHC) space through a transformation of variables allows unique recovery of the observationally-constrained joint distribution for the two model parameters, from which the marginal distribution of ECS can readily be derived. The method is extended to provide estimated distributions for Transient Climate Response (TCR). The AW distributions from the two D&A studies produce almost identical results. Combining the two sets of results provides best estimates [5–95% ranges] of 1.66 [0.7 – 3.2] K for ECS and 1.37 [0.65 – 2.2] K for TCR, in line with those from several recent studies based on observed warming from all causes but with tighter uncertainty ranges than for some of those studies. Almost identical results are obtained from application of an alternative profile likelihood statistical methodology.

Keywords: climate sensitivity · transient climate response · effective ocean diffusivity attributable warming · AR5 · profile likelihood

[1] *Corresponding author address*: Bath, United Kingdom.
E-mail: nhlewis@btinternet.com

1. Introduction

Climate sensitivity is a key metric of the climate system's response to changes in radiative forcing. 'Equilibrium climate sensitivity' (ECS) is a measure of the change in global mean surface temperature (GMST), after the ocean has equilibrated, in response to a doubling of atmospheric CO_2 concentration. 'Transient climate response' (TCR) is a shorter-term metric of sensitivity, representing the theoretical global warming at the end of an approximately 70-year period over which CO_2 concentration, rising by 1% per annum, doubles. Uncertainty in ECS and TCR have proved difficult to reduce, with the IPCC's Fifth Assessment scientific report (AR5) giving a range of 1.5–4.5 K for ECS, the same as in most scientific assessments over the previous three decades, and of 1.0–2.5 K for TCR (Collins et al, 2014). Uncertainty in aerosol forcing is the major obstacle to reducing uncertainty in observationally-based ECS and TCR estimates (Lewis and Curry 2014).

A number of recent instrumental-observation based studies employing simpler models (e.g. Aldrin et al. 2012; Schwartz 2012; Otto et al. 2013; Lewis 2013; Masters 2014; Skeie et al. 2014; Lewis and Curry 2014) have pointed to lower ranges for ECS and TCR than those exhibited by ensembles of 3D global climate models (GCMs). The models they used vary in complexity from zero-dimensional global energy-balance models (EBMs) through hemispherically-resolving models, to 2D GCMs. This study estimates ECS and TCR using 3D GCM-derived estimates of global surface warming attributable to well-mixed greenhouse gases (GHGs), scaled to best match observed warming patterns, in an attempt to overcome some limitations of studies that employ less complex climate models.

Instrumental-observation based sensitivity studies usually compare modelled and observed changes in surface temperatures and other climate variables over much or all of the period for which reasonable surface temperature data exists, since circa 1850 (the instrumental period). A major challenge for such studies is separating out and thereby quantifying the relative effects of GHGs and other forcing agents, in particular anthropogenic aerosol forcing, which is very uncertain. (The term 'forcing' is used to refer to effective radiative forcing (ERF), as defined in AR5 (Myhre et al 2014).) The best-estimate aerosol and GHG global forcing time series given in AR5 (Table AII.1.2: Prather et al 2014) have an almost perfect negative correlation of −0.98 over 1850–2011. Attempts to separate and quantify the effects of aerosol forcing, GHG forcing and other causes of temperature changes during the instrumental period are sensitive to analysis period when using models employing only global mean data (e.g. Imbers et al. 2013, Table 1), reflecting the confounding effects of multidecadal internal variability. Climate sensitivity studies involving model-to-observation comparisons resolved by latitude band (Libardoni and Forest 2011; Lewis 2013) or by hemisphere (Aldrin et al 2012; Ring et al. 2012; Skeie et al. 2014) are better able to separate out the effects of aerosol forcing. This is because the estimated latitudinal and hemispherical distribution of aerosol forcing differs from that of GHGs. Such studies normally require multiple runs of the climate model involved with varying combinations of model parameter values so as to explore a wide range of possible values for key uncertain climate system

properties, in particular climate sensitivity, aerosol forcing and ocean heat uptake efficiency. This makes it computationally very expensive to use a 3D GCM. Moreover, there may be combinations of such properties that a GCM is unable to explore because of its structural limitations. For example, HadCM3 (Gordon et al. 2000) appears to have difficulty exploring most of the region of aerosol-forcing–ECS space that is consistent with observations and AR5 Table AII 1.2 forcing estimates (Harris et al. 2013, Figure S2).

Pattern-based detection and attribution studies (henceforth "attribution studies") offer an alternative way of using 3D GCMs to separate out the effects of GHG forcing from other anthropogenic (OTH) forcing and from natural solar and volcanic (NAT) forcing. Attribution studies involve simulation runs with different categories of forcing but standard model parameter settings. Phase 5 of the Coupled Model Intercomparison Project (CMIP5; Taylor et al. 2012) specifies simulations that include only GHG forcing and only NAT forcing as well as all forcings. Making the usual assumption of linearity of response to forcings, this enables the model response to OTH forcing to be obtained by subtraction. Attribution studies take account of uncertainty due to internal climate variability, estimated from long pre-industrial GCM control runs. They usually employ optimal fingerprint methods (Hegerl et al. 1996; Hasselmann 1997; Allen and Tett 1999; Hegerl and Zwiers 2011) to help separate patterns of forced change from each other and from internal variability.

Attribution studies use multiple-regression techniques to estimate what scaling factors to apply to the GCM-simulated temperature response patterns for the various categories of forcing in order to best match their sum with observational data. The scaling factors (being the regression coefficients) adjust for the GCM(s) under- or over-estimating the responses to the various categories of forcing and/or the forcing strengths. This assumes an approximate linear relationship between ERF and model-simulated warming, which – leaving aside volcanic forcing – seems supportable (Gregory and Forster 2008), at least with respect to the major GHG and sulphate aerosol forcings (Gillett et al. 2004). Estimates of the warming attributable to each forcing category can then be derived, by multiplying the applicable model-simulated temperature gain by its scaling factor. The accuracy of these estimates depends on the different spatiotemporal response patterns for the various categories of forcing being realistically represented in the GCM(s), and separable from each other and from internal variability patterns. If a particular forcing has a different response pattern from that of other forcings in the same category, its omission or substantial misrepresentation in the GCM(s) is likely to bias estimation.

As mentioned previously, there is a very high absolute correlation between the evolution of GHG and of aerosol forcing. The same applies between GHG and OTH forcing, which in most GCMs is dominated by aerosol forcing, with smaller contributions from ozone, land use, stratospheric water vapour and other minor forcings. Therefore, multidecadal internal variability – which noticeably affects surface temperature even at hemispherical and global scales – may be a confounding factor for separating estimation of the OTH and GHG scaling factors in attribution studies, which depend on global mean as well as spatial information. The potential severity and

analysis-period dependency of this problem is evident from a simple attribution analysis based on synthetic GMST data incorporating a small fluctuation in line with an index representing the Atlantic Multidecadal Oscillation (AMO: Enfield et al. 2001) (see Supplementary Material: S1). Gillett et al. (2012) found that using data from the twentieth-century, the first two decades of which coincided with an AMO cycle bottom and were anomalously cool, introduced substantial upwards bias into estimation of the GHG scaling factor relative to estimation based on the longer 1851–2010 period. Estimation based on 1901–2010 data showed only a minor upwards bias. This suggests that attribution analyses based on data for 1851–2010, 1901–2010 or similarly long periods should be used for estimating global surface warming attributable to GHG (AW).

Notwithstanding uncertainty arising from mismatches between GCM simulations and the climate system, one can treat observationally-constrained attribution study AW estimates as "observables", using them in the same way as observed temperature changes. However, attribution studies do not normally seek to estimate ocean heat uptake – which largely determines the relationship between ECS and warming over the instrumental period – and hence do not in themselves enable observationally-based estimation of ECS. Nevertheless, it is possible to achieve such estimation by combining an attribution study's AW estimate with an observationally-based estimate of effective heat capacity (EHC) – the global ratio of planetary heat uptake, predominantly by the ocean, to the change in surface temperature over a multidecadal period. Those observationally-based estimates for AW and EHC can then be compared with values simulated by a simple GHG-forced EBM with adjustable parameters for ECS and effective ocean diffusivity (Frame et al. 2005; Allen et al. 2009; Lewis 2014). That approach is used in this study.

Lewis (2014) showed that, given the error distribution assumptions made, a unique estimated posterior distribution for ECS was obtained upon carrying out a transformation of variables followed by the standard Bayesian procedure of integrating out the unwanted model parameter (effective ocean diffusivity), and that results upon doing so agreed well with estimation using a non-Bayesian profile likelihood method. The transformation-of-variables approach presented in Lewis (2014) and closely followed here is objective: it is intended not to incorporate any prior knowledge of the values of the parameters to be estimated. I use the same global energy balance model as in that study, but based on GCM multimodel mean AW estimates for the longest available analysis periods from two recent attribution studies, along with updated estimates for EHC and the evolution of greenhouse gas forcing, using data from AR5. The method is extended to provide an estimated distribution for TCR as well as for ECS.

The material is organized as follows. Section 2 outlines the methods used, and deals with data selection, uncertainty assessment and processing. Section 3 sets out the results. Section 4 discusses the results and relevant related issues.

2. Methods and Data

a. Methods

The method for estimating ECS is essentially identical to that used in Lewis (2014). The main statistical approach is an objective Bayesian one. Results using a frequentist profile likelihood method are also given.

The method involves comparing EBM-simulated and estimated actual values of "observables" – climate variables that can be fully constrained by observational data, thereby providing observationally-based estimates for them. The observables used are AW – the linear trend GMST increase attributable to greenhouse gases, denoted by $T_{A,}$ and effective heat capacity (EHC), denoted by C_H. Observationally-based estimates of AW and EHC are respectively obtained from attribution analyses, and estimated from the ratio of observed changes in ocean heat content and in GMST. The EBM uses given values of climate sensitivity (S) and effective ocean vertical heat diffusivity (K_v), and data consisting of a time series of estimated GHG forcing, to simulate global surface temperature and ocean heat content changes attributable to GHG forcing from 1850 to 2010, from which AW and EHC values are derived. Further method details are given in Appendix A.

The method used in Lewis (2014) is extended here to encompass estimation of TCR as well as ECS. The TCR values arising from each (S, K_v) combination, and hence the (TCR, K_v) combinations corresponding to every (T_A, C_H) combination, are calculated from a second set of EBM simulations. In these simulations, forcing increases linearly, replicating the doubling of CO_2 concentration over 70 years in the 1% yr^{-1} increasing CO_2 experiment specified in the TCR definition. A PDF for TCR is then derived using the same method as for ECS. This method of estimating TCR is considered more accurate than estimating it directly from AW since, although the TCR estimate will mainly reflect the relationship of AW to the increase in GHG forcing over the relevant period, the relationship between TCR and AW varies somewhat between GCMs.

b. Effective heat capacity estimate: data selection, uncertainty assessment and processing

EHC is derived as the ratio of the change in observationally-estimated climate system heat content, ΔHC, to the change in GMST, ΔT_G. As in Frame et al. (2005) and Lewis (2014), the change in heat content is measured between 11 year means at the beginning and end of the period covered by the heat content data, that is between 1958–1968 and 2001–2011. Doing so gives a central estimate (calculated from the data underlying Box 3.1, Figure 1) for ΔHC of 203.7 zeta joules (ZJ), or 0.400 GJm^{-2} over the Earth's surface; the change derived from applying the 1958–2011 linear regression trend over 43 years is similar. It is desirable to use well-separated averaging periods, each a decade or more long, so as to minimise the impact of internal variability and measurement error.

Although heat uptake by the non-abyssal ocean is dominant, minor contributions from the abyssal ocean, ice melt, land and atmosphere are included. The data used correspond to the observational best estimates and uncertainty ranges for energy accumulation in the climate system shown in Box 3.1, Figure 1 of AR5 (Rhein M et al, 2014). Whilst over some shorter periods the various OHC datasets disagree, for the long 1958–2011 period there is good agreement between the 0–2000 m OHC change estimate per AR5 Box 3.1, an estimate using Levitus et al. (2012) data for 0–700 m as well as for 700–2000 m depths, and one based on the Lyman and Johnson (2014) estimate for 0–1800 m depth.

A conservative approach is taken regarding heat-content uncertainty. For each 11-year period, the mean of the AR5 Box 3.1 Figure 1 annual observational uncertainty estimates (which assume a Gaussian distribution) for each year in the period is taken, without assuming any degree of uncertainty independence within each period. This approach is taken mainly on account of the likelihood of there being substantial persistent common error elements within each period, for example from instrumentation and sampling biases. A secondary reason is that it provides an allowance for internal variability in ΔHC (estimated, from the long HadCM3 control run, to be minor in relation to observational uncertainty) and for any model inaccuracy or other sources of error related to the use of EHC as an observable. Independence of uncertainty in heat content between 1958–68 and 2001–11 is assumed, with the estimated standard deviations for each period added in quadrature to give a standard deviation for ΔHC of 0.129 GJm^{-2}. As discussed in Section 4, ECS estimation is relatively insensitive to any inaccuracy in ΔHC.

The HadCRUT4v2 index (Morice et al. 2012) is used to estimate ΔT_G, the change in GMST between 1958–1968 and 2001–11, as 0.52 K. Uncertainty in ΔT_G is represented by a Gaussian distribution with a standard deviation of 0.088 K. This estimate is derived by adding in quadrature the 1963 and 2006 uncertainty standard deviations for the decadally smoothed HadCRUT4 dataset, and an allowance for internal variability of 0.08 K. This allowance is estimated from years 2100 to 6100 of the long HadCM3 control run.

As in Lewis (2014), an estimated PDF for the true effective heat capacity, C_H^t, is derived by sampling from the error distributions for ΔHC and ΔT_G, and a profile likelihood for C_H^t computed. Details are given in Supplementary Materials: S2.

c. Attributable warming estimates: selection, uncertainty assessment and processing

Three multimodel attribution studies are featured in Chapter 10 of AR5 (Bindoff et al 2014), which deals with detection and attribution: Gillett et al. (2013) (G13); Jones et al. (2013) (J13); and Ribes and Terray (2013) (R13). I do not include R13 AW values in this analysis, since R13 gives no multimodel mean AW estimate. For reasons given earlier, I selected AW estimates from G13 and J13 based on the longest period available: 1861–2010 for G13 and 1901–2010 for J13. Both the J13 and G13 analyses involved the same set of models, save for one more model being used in G13. The G13 and J13 multimodel mean AW estimates that give equal weight to each model are used.

For G13 I use their error-in-variables (EIV) estimate, which uses a regression method that accounts for model uncertainty. For J13 I use their, 'Weighted Avg', estimate, which allows for uncertainty arising from model internal variability.

G13 also gives uncertainty estimates for the product of the GHG regression coefficient and mean model TCR, both with and without taking into account both observational uncertainty and, dominating it, uncertainty in the individual model relationship between TCR and AW. The latter uncertainty is used as a proxy for any model and methodological inaccuracies that are not allowed for in the estimates of regression coefficient and observational uncertainty, and that affect AW in an additive manner. I accordingly increase the uncertainty ranges for the G13 and J13 AW estimates by scaling them by the ratio of the described G13 uncertainty estimates with and without allowance for observational and TCR-to-AW relationship uncertainties. The effects of excluding the resulting one-third increase in uncertainty allowance are discussed in Section 4, and provide a guide to sensitivity of uncertainty in ECS and TCR estimation to uncertainty additively affecting AW.

The uncertainty ranges for the G13 and J13 multimodel AW estimates used are both almost symmetrical about the central estimate and, being based on regression analysis, can be regarded in Bayesian terms as derived from objective posterior PDFs or their integrals, CDFs. Indeed, J13 states that the uncertainty percentiles are derived from a CDF. The 5–95% ranges given are converted into standard deviations on the simplifying assumption that the uncertainty has a Gaussian distribution. Since the estimates of natural internal variability used in attribution studies have a limited number of degrees of freedom (24 for the J13 AW estimate used here, somewhat more for the G13 estimate) a *t*-distribution would arguably be more accurate. However, since the Gaussian distributions are fitted using 5–95% uncertainty ranges, not standard deviations, using a Gaussian distribution instead of a *t*-distribution will have very little impact. Assuming objective statistical methodology, a Gaussian-distributed PDF corresponds to an identical Gaussian likelihood function.

Although AW estimates from attribution studies are stated to be global, they are reconstructed from gridded data that has been masked by the availability at grid-cell level of a record of temperature observations adequate to include the grid cell in the attribution analysis. In order not to bias estimation of ECS and TCR downwards, I adjust the AW estimates to reflect, so far as practicable, the effects of observational masking on geographical coverage. Downwards bias is taken to be attributable entirely to GHG forcing, since forcing from components of OTH (mainly aerosols and ozone) is heavily concentrated in the best-observed latitudes and masking effects should be small. The 'observational' GMST trends (shown in J13 and G13 alongside their AW estimates), which are reconstructed from HadCRUT4 gridded data having the same masking as used in the applicable attribution analysis, are used to estimate bias. An adjustment factor is derived by dividing these 'observational' GMST trends into the unmasked actual HadCRUT4 GMST trends, and then scaling the fractional part of the quotient by the ratio of warming attributed to all causes to AW. The resulting upwards adjustment to AW (which is rounded to a whole percentage) is 6% for J13, and is applied to the AW uncertainty range as well as to its central estimate. It is larger, at 10%, for G13,

consistent with the greater proportion of missing data for an analysis extending back further. Table 1 compares the original and the adjusted AW estimates and uncertainty ranges for each of the attribution studies used.

Table 1 Central estimates and uncertainty ranges for AW before and after multiplicative adjustment to reflect (in both cases) the full HadCRUT4 spatial coverage and (for the uncertainty range only) allowance for any model and methodological inaccuracies not covered by the original uncertainty ranges, for the Gillett et al. (2013) and Jones et al. (2013) studies.

Source of AW estimate	Period over which AW estimated	Original AW central estimate [K]	Original AW uncertainty (standard deviation) [K]	Spatial coverage factor applied to estimate	Multiplier applied to uncertainty range	Adjusted AW central estimate [K]	Adjusted AW uncertainty (standard deviation) [K]
G13	1861-2010	0.85	0.173	1.10	1.333	0.935	0.254
J13	1901-2010	0.83	0.194	1.06	1.333	0.880	0.275

The original AW uncertainty standard deviations have been derived on the stated Gaussian distribution assumption, by dividing the widths of the 5–95% uncertainty ranges provided in the two studies by 3.29, the applicable ratio for this distribution.

d. GHG forcing data: selection, adjustment and allowance for uncertainty

Time series for greenhouse gas ERFs are sourced from Table AII.1.2 of AR5, combining the CO2 and Other GHG values. Two models used in the attribution studies involved, CNRM-CM5 and NorESM1-M, included ozone forcing in their Historical GHG simulations, despite it not being a well-mixed greenhouse gas. To allow for inclusion of ozone in those two models, the GHG time series presented in AR5 Table AII.1.2 was adjusted up by 4% in all years. See Supplementary Materials: S2 for details.

The CO_2 forcing time series given in AR5 Table AII.1.2 is based on an $F_{2\times CO2}$ value of 3.71 Wm^{-2}. Therefore, that value for $F_{2\times CO2}$ is used in the EBM simulations.

Since the evolution of CO_2 and the other main greenhouse gases over the period involved is accurately known in terms of concentration, and ECS and TCR are defined in terms of the effect of a change in concentration of CO_2, GHG forcing uncertainty has a relatively limited impact. This assumes, as in AR5 (Myhre et al, 2014), perfect correlation across all greenhouse gases of uncertainty in the relationship between concentration and ERF. On that basis, whilst uncertainty in recent ERF from GHG is considerable, its uncertainty relative to the ERF from a doubling of CO_2 concentration, $F_{2\times CO2}$, is small. Accordingly, since the value of $F_{2\times CO2}$ used in the EBM to convert ECS to the climate feedback parameter ($F_{2\times CO2}$/ECS) is the same as the value used in the derivation of the GHG forcing series it uses, uncertainty in GHG ERF has relatively little effect on the amount of warming simulated by the EBM and hence on ECS estimation. It does have a modest impact, since for any given (S, K_v) combination and

change in GHG concentration, the ratio of climate-system heat uptake to the total change in forcing will vary with $F_{2\times CO2}$.

Table 2 Best estimates (medians) and uncertainty ranges for ECS and TCR derived, upon integrating out K_v, using the transformation of variables method.

Source of AW estimate	Method employed	ECS best estimate [K]	ECS 17-83% range [K]	ECS 5-95% range [K]	TCR best estimate [K]	TCR 17-83% range [K]	TCR 5-95% range [K]
G13	Transformation of variables	1.68	1.15–2.40	0.80–3.10	1.39	1.00–1.80	0.75–2.15
G13	*Profile likelihood*	*1.69*	*1.15–2.40*	*0.80–3.10*			
J13	Transformation of variables	1.64	1.05–2.40	0.70–3.20	1.36	0.95–1.80	0.65–2.20
J13	*Profile likelihood*	*1.64*	*1.05–2.40*	*0.70–3.20*			

Results shown are based on AW estimates from the Gillett et al. (2013) and Jones et al. (2013) studies, adjusted to reflect the full HadCRUT4 spatial coverage. Ranges are stated to the nearest 0.05 K. The lines in italics show, for ECS, the comparable results using the SRLR profile likelihood method; the best estimate represents the likelihood peak.

Although the conversion by GCMs of GHG concentrations to ERF values also involves uncertainties, that should not affect the AW estimate derived from an attribution study. Any under- or over-estimates by the GCMs used in G13 and J13 of the ERF arising from the specified CMIP5 GHG-concentration time series should, if they bias the GCM-simulated GHG-induced warming, be reflected in the GHG scaling factor.

In the light of these considerations, a Gaussian-distributed GHG-forcing uncertainty allowance with a 5–95% range of ±10%, half that given in AR5 Table 8.6 (Myhre at al 2014) for GHG ERF, appears adequate. However, given the two-stage (attribution analysis, then EBM-simulation based) method used to estimate ECS and TCR, model inaccuracies and other error sources are likely to exist. Separate allowance for model and methodological uncertainties having additive effects on AW has been made, as discussed in subsection (c). However, some uncertainties may, like forcing uncertainty, have a divisive effect on AW or otherwise divisively affect the final estimate. Whilst it is difficult to determine what, if any, additional allowance is appropriate for these, ±20% (Gaussian 5–95% range), added in quadrature to the allowance for forcing uncertainty, is judged to be generous. The primary results presented are with such an allowance being made (which has the same effect as increasing the allowance for forcing uncertainty from ±10% to ±22%); the results without it are also shown. Following Lewis (2014), allowance for forcing and other divisive uncertainty is reflected in the PDF for the true value of AW, T_A^t, by computing

a histogram of the quotients of pairs of samples from the error distributions for the adjusted AW estimate and (centred at unity) for forcing and similar uncertainty, in the same way as for EHC. A profile likelihood for AW is also derived, as for EHC.

3. Results

Best estimates and uncertainty ranges for ECS and TCR derived from the adjusted G13 and J13 AW estimates, in combination with the observationally-derived EHC estimate, are set out in Table 2. Marginal posterior PDFs for ECS are shown in Figure 1. The box plots at the bottom of Figure 1 show graphically the same information as in Table 2. The ECS values in italics in Table 2, corresponding to the dashed-line box plots in Figure 1, are derived using the alternative profile likelihood method. They are almost identical to the results obtained using the transformation of variables method, which represent objective Bayesian one-sided credible interval percentage points derived from the marginal posterior PDFs plotted in Figure 1. This confirms the frequentist validity of both methods in this case.

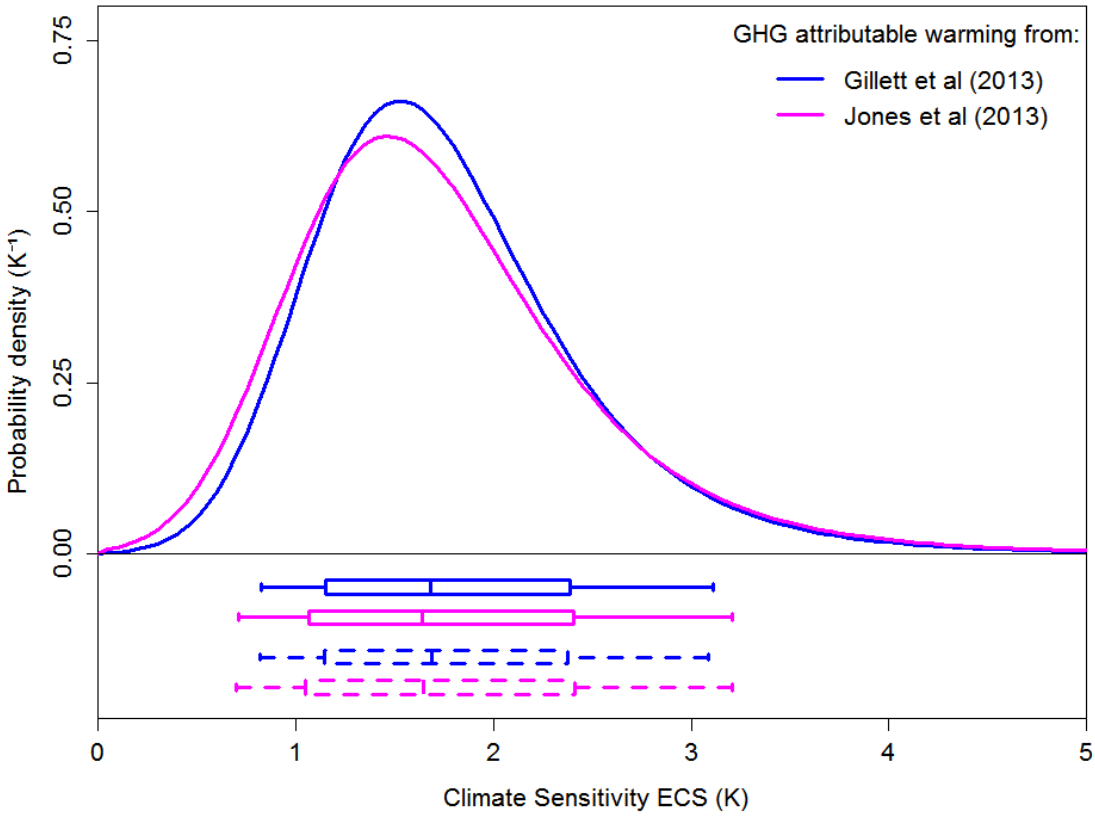

Fig. 1. Estimated marginal PDFs for climate sensitivity derived, upon integrating out K_v, using the transformation of variables method. The box plots indicate boundaries, to the nearest grid value, for the percentiles 5–95 (vertical bar at ends), 17-83 (box-ends), and 50 (vertical bar in box), and allow for off-graph probability lying between $S = 5$ K and $S = 20$ K. Solid line box plots reflect the percentile points of the CDF corresponding to the plotted PDF. Dashed line box plots give confidence intervals derived using the SRLR profile likelihood method (the vertical bar in the box showing the likelihood profile peak).

For ECS, the best estimate based on the J13 AW estimate, at 1.64 K, is almost the same as the 1.68 K best estimate based on the G13 AW estimate. The mean of the best estimates from the two attribution studies is 1.66 K. The ECS uncertainty ranges using the two AW estimates are almost coincident, the G13-based ECS uncertainty ranges being marginally narrower with a 5–95% range of 0.8–3.1 K against 0.7–3.2 K for J13 (ranges being rounded to the nearest 0.05 K). The overall 17–83% range, taking the outermost G13- and J13-based values from both methods, is 1.05–2.4 K.

Marginal posterior PDFs for TCR and related box plots are shown in Figure 2. The TCR best estimates derived from the J13 and G13 AW estimates are also almost identical, at 1.36 K and 1.39 K respectively, with a mean best estimate of 1.37 K. As for ECS, marginally narrower TCR ranges are obtained using the G13 rather than the J13 AW estimate. Taking the outermost G13- and J13-based values, the overall 17–83% range is 0.95–1.8 K, whilst the 5–95% range is 0.65–2.2 K.

Sensitivity of ECS estimation to variation in the central estimate of EHC, whether caused by inaccuracy in estimation of ΔHC or of ΔT_G, was investigated and found to be small. A 10% increase in the ΔHC or ΔT_G central estimate (broadly, respectively increasing or decreasing the central EHC estimate pro rata) respectively increased or reduced the best estimate for ECS by 2%. The effect of such changes in EHC on TCR estimation was negligible.

Best estimates and uncertainty ranges for effective ocean vertical heat diffusivity, in terms of its square root K_v, were found to be the same whether using the J13 or G13 AW estimates, and whether obtained by undertaking a transformation of variables and then integrating out S or by using the profile likelihood method. The best estimate for K_v is 0.53 cm $s^{-0.5}$, with 17–83% and 5–95% ranges of respectively 0.3–0.8 cm $s^{-0.5}$ and 0.15–1.0 cm $s^{-0.5}$.

Alternative results omitting the ±20% (5–95% range) allowance made for possible model and other inaccuracies that have a divisive effect on AW, as discussed in Section 2(d), differ as follows from the main results. For both ECS and TCR, best estimates are unchanged, as are the lower bounds of all the uncertainty ranges (changes in bounds are to the nearest 0.05 K). The 83% and 95% bounds for ECS reduce by respectively 0.1 K and 0.25 K; those for TCR reduce by respectively 0.05 K and 0.15 K. Changes are the same whether using the G13 or J13 AW estimate, and whether using the main or the profile likelihood method. The relatively modest magnitude of these changes shows that uncertainty in ECS and TCR estimation is not particularly sensitive to possible model and other inaccuracies that have a divisive effect on estimation of AW.

Excluding instead the one-third increase made in the allowance for uncertainty having an additive effect on AW, as discussed in Section 2(c), again leaves best estimates unchanged, but has less asymmetrical effects on uncertainty, with 5%, 17%, 83% and 95% bounds for ECS changing by respectively +0.15 K, +0.1 K, −0.1 K and −0.25 K from the main results values when using the G13 AW estimate and either the main or the profile likelihood method. Changes when using the J13 AW estimate are

broadly similar, although less consistent between the main and the profile likelihood methods. The 5%, 17%, 83% and 95% bounds for TCR change by respectively +0.1 K, +0.05 K, −0.05 K and −0.1 K from the main results values when using the J13 AW estimate, and slightly more when using the G13 AW estimate.

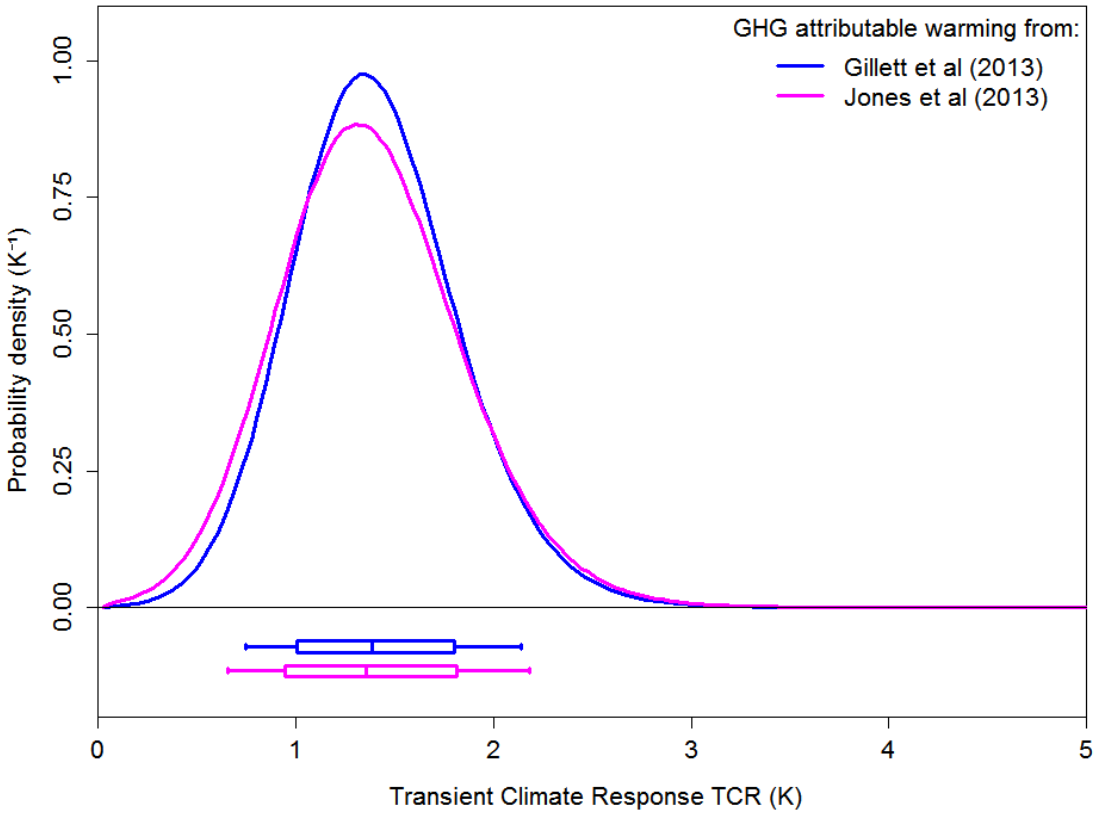

Fig. 2: Estimated marginal PDFs for transient climate response derived, upon integrating out K_v, using the transformation of variables method. The box plots indicate boundaries, to the nearest grid value, for the percentiles 5–95 (vertical bar at ends), 17-83 (box-ends), and 50 (vertical bar in box). They reflect the percentile points of the CDF corresponding to the plotted PDF.

4. Discussion

The ECS and TCR best estimates obtained here lie towards the bottom ends of the AR5 'likely' (66%+ probability) ranges, being 1.5–4.5 K for ECS and 1–2.5 K for TCR. The upper bounds of these ranges substantially exceed the 17–83% ranges given in Table 2. However, this study's results are very similar to those obtained in a number of recent studies that are based on warming – both of the global surface and in the body of the ocean – over the bulk of the instrumental period. Such studies include those (Aldrin et al. 2012; Ring et al. 2012; Lewis 2013; Skeie et al. 2014) that form their own inverse estimates for aerosol forcing – the dominant source of uncertainty when ECS and TCR estimation is based on the AR5 (Myhre et al 2014) forcing estimates. Those four studies all use spatiotemporal temperature data (not just GMST) to estimate aerosol forcing,

and provide results that are not significantly biased upwards by use of an unsuitable estimation period or highly informative prior distributions.

Results from recent energy budget studies (Otto et al. 2013; Lewis and Curry 2014) that use aerosol forcing estimates from AR5 (Myhre et al 2014) or that are similar thereto also give ECS and TCR best (median) estimates in line with those obtained here, but with somewhat higher 95% bounds for ECS. Moreover, ECS median estimates from Aldrin et al. (2012), Otto et al. (2013), Skeie et al. (2014) and Lewis and Curry (2014) using alternative analysis periods ending at the start of this century were very little different from their main estimates, whilst the Lewis (2013) main estimate used data ending in 2001. It follows that the surface temperature 'hiatus' is not responsible for their ECS and TCR estimates being towards the lower end of the AR5 'likely' ranges. Accordingly, evidence from observed warming over the instrumental period now appears to point towards best estimates for ECS and TCR in the region of those reported here, and to upper uncertainty bounds – particularly for ECS – that are lower than those given in AR5.

In a model-based study, Shindell (2014) postulated that spatially inhomogeneous forcings, principally from aerosols and ozone, might lead to substantial underestimation of TCR by global energy budget calculations and similar methods. ECS estimation would also be affected. Results from the present study and from Lewis (2013) – which used a model and data that were latitudinally-resolved – should be unaffected by such concerns. The similarity of their climate sensitivity estimates and those from recent global energy budget studies suggests that the effect of inhomogeneous forcings on global energy budget estimates of TCR and ECS is very minor for the real climate system.

The lower and better-constrained estimate for ECS in this study (median 1.66 K, 5–95% range 0.7–3.2 K) than in Lewis (2014) (median 2.2 K, 5–95% range 1.2–4.5 K) principally reflects the use of attributable warming estimates from much more recent attribution studies. The attribution study from which the AW estimate used in Lewis (2014) was taken used data from the twentieth century, which has been found significantly to bias upwards estimation of the GHG regression coefficient (Gillett et al 2012).

As with most studies that estimate ECS using instrumental period data, strictly it is effective climate sensitivity (a measure of the strengths of climate feedbacks during a period of transient climate change) that is estimated here rather than equilibrium climate sensitivity. Equilibrium climate sensitivity can only be determined once the ocean – but conventionally not ice sheets and other slow components of the climate system – has reached equilibrium. In AR5 it is pointed out (Box 12.2: Collins et al 2014) that in some global climate models equilibrium climate sensitivity is higher than effective climate sensitivity because the feedbacks that are represented in the models (water vapour, lapse rate, albedo and clouds) vary with the climate state. The increase in model sensitivity has been linked to time-varying patterns of temperature increase (Armour et al. 2013) and ocean-heat uptake (Rose et al. 2014). These and similar findings depend on model latitudinal feedback patterns and ocean and cloud behaviour, which vary substantially

between coupled GCMs (Zelinka and Hartmann 2012; Huang and Zhang 2014). Andrews et al. (2014) found that in most of the CMIP5 models the incremental climate feedback parameter reduces (i.e. effective climate sensitivity increases) somewhat on a multidecadal timescale when CO_2 levels are abruptly quadrupled. However, Forster and Taylor (2006) found that most of the 20 previous-generation models they studied showed no evidence of a change in climate feedback parameter over 200+ year simulations forced by a CO_2 levels ramped upwards at 1% yr^{-1} and stabilised after 70 years. It is unclear whether effective climate sensitivity will increase over time in the real climate system under realistic forcing scenarios.

The best estimate of 0.53 cm $s^{-0.5}$ obtained here for effective ocean vertical heat diffusivity, in terms of its square root K_v, is very close to the value of ~0.55 cm $s^{-0.5}$ given by both Aldrin et al. (2012) and Ring et al. (2012), studies that also use relatively simple ocean models. Aldrin et al. (2012) give a narrower uncertainty range for K_v than that obtained here; Ring et al. (2012) do not provide uncertainty ranges.

Acknowledgements. I thank Gregory Johnson for supplying the data underlying Box 3.1, Figure 1 of AR5, Gareth Jones for supplying numerical results and other information relating to Jones et al (2013), and Judith Curry, Jonathan Jones and Paul Kirwan and two reviewers for helpful comments that significantly improved the manuscript.

Appendix A

Further details of method used to estimate ECS

As stated in Section 2, the method closely follows that in Lewis (2014). One observable used, T_A, represents the estimated GMST change over the full analysis period attributable to greenhouse gases, based on the linear trend in GMST from the simulated response to GHG-only forcing. In the case of the observationally-constrained estimate of T_A, derived from GCM simulations, the simulated linear trend has been scaled by the GHG regression coefficient estimated in the attribution analysis. The EBM-simulation trend estimate of T_A is unscaled. The other observable, effective heat capacity C_H, is taken to be the same for GHG-only forcing as it is for historical warming (Frame et al 2006). Model accuracy is assumed, with there being a 'true' setting (S^t, K_v^t) of model parameters that simulates 'true' (error-free) values (T_A^t, C_H^t). Estimated (posterior) probability density functions (PDFs) for the true values of the observables (those that would have been observed in the absence of error and internal variability), $p_{T_A^t}(T_A)$ and $p_{C_H^t}(C_H)$, are derived respectively from the uncertainty ranges given in the relevant attribution analysis and from observational data error distributions, as described in Section 3. Since C_H is a measure of heat capacity, it should be independent of the change in GMST and hence of T_A. The joint density for T_A and C_H, $p_{T_A^t, C_H^t}(T_A, C_H)$, is accordingly obtained by multiplying their individual densities. As the EBM is a deterministic rather than a statistical model, the dispersion of the estimated PDFs for S must entirely reflect uncertainties in the observationally-constrained estimates of T_A and C_H.

The EBM used has a diffusive ocean below a 75-m-deep mixed layer (Andrews and Allen 2008, equation 8). EBM simulations are run using all parameter value combinations lying on a grid that is uniformly spaced in terms of S and K_v and sufficiently large for there to be negligible probability of the true values of S or K_v lying outside it. Four hundred values of S from 0.05 to 20 K, and sixty values of K_v from 0 to 2.95 cm $s^{-0.5}$, were used. For notational convenience, here K_v represents the square root of effective ocean vertical diffusivity, which controls C_H in an approximately linear manner (Sokolov et al. 2003). The annual EBM-simulation time series are used to compute T_A^m and C_H^m. T_A^m is calculated as the linear-regression-based change in modelled global surface temperature over the period used in the relevant attribution analysis (that is, the product of the regression trend per annum and the length of the period in years). C_H^m is calculated as the ratio of changes in modelled ocean heat content and global temperature between the means of 11-year periods centred on 1963 and 2006, thus using data spanning 1958–2011, the period covered by the observational data used.

The observables and parameters are both bivariate and, with the EBM being deterministic, the model T_A^m and C_H^m values are smooth differentiable functions of the

parameters. Moreover, each pair of $(T_{\mathrm{A}}^{m}, C_{\mathrm{H}}^{m})$ values corresponds to a unique pair of $(S^{\mathrm{m}}, K_{\mathrm{v}}^{\mathrm{m}})$ values and vice-versa. Accordingly, there is an invertible both-ways differentiable one-to-one relationship between joint model parameter settings, $(S^{\mathrm{m}}, K_{\mathrm{v}}^{\mathrm{m}})$, and joint values of $(T_{\mathrm{A}}^{m}, C_{\mathrm{H}}^{m})$. Given the assumption of model accuracy the same relationship exists between the true joint values $(T_{\mathrm{A}}^{\mathrm{t}}, C_{\mathrm{H}}^{\mathrm{t}})$ and $(S^{\mathrm{t}}, K_{\mathrm{v}}^{\mathrm{t}})$. The estimated joint posterior PDF for $(S^{\mathrm{t}}, K_{\mathrm{v}}^{\mathrm{t}})$ is therefore directly and uniquely related to that for $(T_{\mathrm{A}}^{\mathrm{t}}, C_{\mathrm{H}}^{\mathrm{t}})$ through the standard formula (Mardia et al. 1979) for converting PDFs upon a transformation of variables:

$$p_{S^{\mathrm{t}},K_{\mathrm{v}}^{\mathrm{t}}}(S, K_{\mathrm{v}}) = p_{T_{\mathrm{A}}^{\mathrm{t}},C_{\mathrm{H}}^{\mathrm{t}}}(f(S, K_{\mathrm{v}}))\, J_f \tag{1}$$

where *f* is the functional relationship between $(S^{\mathrm{m}}, K_{\mathrm{v}}^{\mathrm{m}})$ and $(T_{\mathrm{A}}^{\mathrm{m}}, C_{\mathrm{H}}^{\mathrm{m}})$ and J_f is the absolute Jacobian determinant, given by:

$$J_f = \text{absolute value of} \left\| \begin{pmatrix} \dfrac{\partial T_{\mathrm{A}}^{\mathrm{m}}}{\partial S^{\mathrm{m}}} & \dfrac{\partial T_{\mathrm{A}}^{\mathrm{m}}}{\partial K_{\mathrm{v}}^{\mathrm{m}}} \\ \dfrac{\partial C_{\mathrm{H}}^{\mathrm{m}}}{\partial S^{\mathrm{m}}} & \dfrac{\partial C_{\mathrm{H}}^{\mathrm{m}}}{\partial K_{\mathrm{v}}^{\mathrm{m}}} \end{pmatrix} \right\|_{S^{\mathrm{m}}=S, K_{\mathrm{v}}^{\mathrm{m}}=K_{\mathrm{v}}} \tag{2}$$

The EBM simulations provide the values of $(T_{\mathrm{A}}^{\mathrm{m}}, C_{\mathrm{H}}^{\mathrm{m}})$ at each $(S^{\mathrm{t}}, K_{\mathrm{v}}^{\mathrm{t}})$ combination, and hence the form of *f* and, by numerical differentiation, of J_f. Once the joint posterior PDF for $(S^{\mathrm{t}}, K_{\mathrm{v}}^{\mathrm{t}})$ has been calculated, a marginal PDF for S^{t} is obtained by integrating out K_{v}, following standard Bayesian methodology. Uncertainty ranges reflect the percentile points of the corresponding cumulative probability distribution function (CDF), and are termed credible intervals.

The frequentist validity, in terms of repeated sampling properties, of the credible intervals provided by the main objective Bayesian method is checked by also deriving confidence intervals for *S* using a profile-likelihood approach (Allen et al. 2009). Profile likelihood is an alternative objective parameter inference method giving confidence intervals with at least approximate frequentist validity (Pawitan 2001). Profile likelihoods for AW and EHC are derived, and multiplicatively combined to form a joint (AW, EHC) likelihood. That joint likelihood is then restated in (S, K_v) coordinates (likelihoods, unlike PDFs, being unaffected by a change in variables), and the profile likelihood for *S* computed. Confidence intervals are then calculated using the signed root log-likelihood ratio (SRLR) method.

References

Aldrin M, Holden M, Guttorp P, Skeie RB, Myhre G, Berntsen TK (2012) Bayesian estimation of climate sensitivity based on a simple climate model fitted to observations of hemispheric temperatures and global ocean heat content. *Environmetrics* 23:253-271

Allen MR, Tett SFB (1999) Checking for model consistency in optimal fingerprinting. Clim. Dyn., 15, 419–434.

Allen MR, Stott PA (2003) Estimating signal amplitudes in optimal fingerprinting. Part I: Theory. Clim. Dyn., 21, 477–491.

Allen MR, Frame DJ, Huntingford C, Jones CD, Lowe JA, Meinshausen M, Meinshausen N (2009) Warming caused by cumulative carbon emissions towards the trillionth tonne. *Nature*, 458, 1163–6.

Andrews DG, Allen MR (2008) Diagnosis of climate models in terms of transient climate response and feedback response time. *Atmos. Sci. Lett*., 9, 7–12

Andrews T, Gregory JM, Webb MJ (2014) The dependence of radiative forcing and feedback on evolving patterns of surface temperature change in climate models. J Clim, 28, 1630–48.

Armour KC, Bitz CM, Roe GR (2013) Time-varying climate sensitivity from regional feedbacks. J Clim 26:4518–4534

Bindoff, Nathaniel L, Stott Peter A et al (2014) Detection and Attribution of Climate Change: from Global to Regional. *Climate Change 2013: The Physical Science Basis Contribution of Working Group I to the Fifth Assessment Report of the Intergovernmental Panel on Climate Change*. Cambridge University Press.

Collins, M, Knutti R et al (2014) Long-term Climate Change: Projections, Commitments and Irreversibility. *Climate Change 2013: The Physical Science Basis Contribution of Working Group I to the Fifth Assessment Report of the Intergovernmental Panel on Climate Change*. Cambridge University Press.

Domingues, CM, Church JA, White NJ, Gleckler PJ, Wijffels SE, Barker PM, Dunn JR (2008) Improved estimates of upper-ocean warming and multi-decadal sea-level rise. Nature 453:1090–3

Enfield DB, Mestas-Nunez AM, Trimble PJ (2001) The Atlantic Multidecadal Oscillation and its relationship to rainfall and river flows in the continental US. Geophys Res Lett 28:2077-2080

Forster, PM de F, Taylor KE (2006) Climate forcings and climate sensitivities diagnosed from coupled climate model integrations. *J. Clim*., 19, 6181–6194.

Frame DJ, Booth BBB, Kettleborough JA, Stainforth DA, Gregory JM, Collins M, Allen MR (2005) Constraining climate forecasts: The role of prior assumptions. *Geophys. Res. Lett*., 32, L09702, doi:10.1029/2004GL022241.

Frame DJ, Stone DA, Stott PA, Allen MR (2006) Alternatives to stabilization scenarios. *Geophys. Res. Lett.*, 33, L14707, doi:10.1029/2006GL025801.

Gillett, NP, Wehner, MF, Tett, SFB, Weaver, AJ (2004) Testing the linearity of the response to combined greenhouse gas and sulfate aerosol forcing. *Geophys. Res. Lett*., 31, 14, L14201, pp. 1-4, doi: 10.1029/2004GL020111

Gillett NP, Arora VK, Flato GM, Scinocca JF, von Salzen K (2012) Improved constraints on 21st-century warming derived using 160 years of temperature observations. *Geophys. Res. Lett*., 39, L01704, doi:10.1029/2011GL050226.

Gillett NP, Arora VK, Matthews D, Stott PA, Allen MR (2013) Constraining the ratio of global warming to cumulative CO2 emissions using CMIP5 simulations. J. Clim., doi:10.1175/JCLI-D-12–00476.1

Gordon C, Cooper C, Senior CA, Banks H, Gregory JM, Johns TC, Mitchell JFB, Wood RA (2000) The simulation of SST, sea ice extents and ocean heat transports in a version of the Hadley Centre coupled model without flux adjustments. *Climate Dynamics*, 16, 147-168.

Gregory JM, Forster PM (2008) Transient climate response estimated from radiative forcing and observed temperature change. J. Geophys. Res. 113.

Harris, Glen R, Sexton, David MH, Booth Ben BB, Collins Mat, Murphy James M (2013) Probabilistic projections of transient climate change. Clim. Dyn. 40, 2937-2972. DOI 10.1007/s00382-012-1647-y.

Hasselmann, K (1997) Multi-pattern fingerprint method for detection and attribution of climate change. Clim. Dyn., 13, 601–611.

Hegerl, GC, von Storch S, Hasselmann K, Santer BD, Cubasch U, Jones PD (1996) Detecting greenhouse gas induced climate change with an optimal fingerprint method. *J. Clim*., 9, 2281–2306.

Hegerl G, Zwiers F (2011) Use of models in detection and attribution of climate change. WIREs Clim. Change, 2, 570–591.

Huang Y, Zhang M (2014) The implication of radiative forcing and feedback for meridional energy transport, Geophys. Res. Lett., 41, 1665–1672

Imbers J, Lopez A, Huntingford C, Allen M (2014) Sensitivity of climate change detection and attribution to the characterization of internal climate variability. *J. Climate*, 27, 3477–3491.

Jones GS, Stott PA, Christidis N (2013) Attribution of observed historical near surface temperature variations to anthropogenic and natural causes using CMIP5 simulations. J. Geophys. Res. Atmos., doi:10.1002/jgrd.50239.

Levitus S et al (2012) World ocean heat content and thermosteric sea level change (0-2000m) 1955-2010. Geophys Res Lett 39:L10603

Lewis N (2013) An objective Bayesian improved approach for applying optimal fingerprint techniques to estimate climate sensitivity. *J. Climate*, 26, 7414-7429.

Lewis N (2014) Objective Inference for Climate Parameters: Bayesian, Transformation-of-Variables, and Profile Likelihood Approaches. *J. Climate*, 27, 7270-7284.

Lewis N, Curry JA (2014) The implications for climate sensitivity of AR5 forcing and heat uptake estimates. *Clim. Dyn.* DOI 10.1007/s00382-014-2342-y

Libardoni AG, Forest CE (2011) Sensitivity of distributions of climate system properties to the surface temperature dataset. Geophys. Res. Lett., 38, L22705, doi:10.1029/2011GL049431.

Lyman JM, Johnson GC (2014) Estimating Global Ocean Heat Content Changes in the Upper 1800 m since 1950 and the Influence of Climatology Choice. J. Climate, 27, 1945–1957.

Mardia KV, Kent JT, Bibby JM (1979) Multivariate Analysis. Academic Press, 518 pp.

Masters T (2014) Observational estimate of climate sensitivity from changes in the rate of ocean heat uptake and comparison to CMIP5 models. Clim Dyn 42:2173-2181 DOI 101007/s00382-013-1770-4

Morice C P, Kennedy JJ, Rayner NA, Jones PD (2012) Quantifying uncertainties in global and regional temperature change using an ensemble of observational estimates: The HadCRUT4 data set. J Geophys Res 117: D08101 doi:101029/2011JD017187

Myhre G, Shindell D et al (2014) Anthropogenic and Natural Radiative Forcing. *Climate Change 2013: The Physical Science Basis Contribution of Working Group I to the Fifth Assessment Report of the Intergovernmental Panel on Climate Change*. Cambridge University Press.

Otto A, Otto FEL, Boucher O, Church J, Hegerl G, Forster PM, Gillett NP, Gregory J, Johnson GC, Knutti R, Lewis N, Lohmann U, Marotzke J, Myhre G, Shindell D, Stevens B, Allen MR (2013) Energy budget constraints on climate response. Nature Geosci 6:415–416

Pawitan Y (2001) In all Likelihood: Statistical Modeling and Inference Using Likelihood Ch. 3.4. Oxford Univ. Press, 514 pp.

Prather M., Flato G, Friedlingstein P, Jones C, Lamarque J-F, Liao H and Rasch P (eds.) (2014) Annex II: Climate System Scenario Tables. *Climate Change 2013: The Physical Science Basis Contribution of Working Group I to the Fifth Assessment Report of the Intergovernmental Panel on Climate Change*. Cambridge University Press.

Rhein M, Rintoul SR et al (2014) Observations: Ocean. *Climate Change 2013: The Physical Science Basis Contribution of Working Group I to the Fifth Assessment Report of the Intergovernmental Panel on Climate Change*. Cambridge University Press.

Ribes A, Planton S, Terray L (2013) Application of regularised optimal fingerprint for attribution. Part II: Application to global near-surface temperature Clim. Dyn., doi:10.1007/s00382-013-1736-6..

Ring MJ, Lindner D, Cross EF, Schlesinger ME (2012) Causes of the global warming observed since the 19th century. Atmos Clim Sci 2:401–415

Schwartz, SE (2012) Determination of Earth's transient and equilibrium climate sensitivities from observations over the twentieth century: strong dependence on assumed forcing. Surveys in geophysics 33.3-4: 745-777.

Shindell, DT (2014) Inhomogeneous forcing and transient climate sensitivity. Nature Clim Chg: DOI: 10.1038/NCLIMATE2136

Skeie RB, Berntsen T, Aldrin M, Holden M, Myhre G (2014) A lower and more constrained estimate of climate sensitivity using updated observations and detailed radiative forcing time series. *Earth Syst Dynam* 5:139–175

Sokolov, AP, Forest CE, Stone PH (2003) Comparing Oceanic Heat Uptake in AOGCM Transient Climate Change Experiments, *J. Climate*, 16, 1573–1582.

Taylor KE, Stouffer RJ, Meehl GA (2012) An overview of CMIP5 and the experiment design. Bull. Am. Meteorol. Soc., 93, 485–498.

Zelinka MD, Hartmann DL (2012) Climate Feedbacks and Their Implications for Poleward Energy Flux changes in a warming climate. J Clim 25:608–624